

Hybridization-Induced Gapped and Gapless States on the Surfaces of Magnetic Topological Insulators

Xiao-Ming Ma^{1*}, Zhongjia Chen^{1*}, Eike F. Schwier^{2*}, Yang Zhang^{3*}, Yu-Jie Hao¹, Rui'e Lu¹, Jifeng Shao¹, Yuanjun Jin¹, Meng Zeng¹, Xiang-Rui Liu¹, Zhanyang Hao¹, Ke Zhang², Wumiti Mansuer², Shiv Kumar², Chunyao Song⁴, Yuan Wang¹, Boyan Zhao¹, Cai Liu¹, Ke Deng¹, Jiawei Mei¹, Kenya Shimada², Yue Zhao¹, Xingjiang Zhou⁴, Bing Shen^{3#}, Wen Huang^{1#}, Chang Liu¹, Hu Xu¹, Chaoyu Chen^{1#}

¹ Shenzhen Institute for Quantum Science and Engineering (SIQSE) and Department of Physics, Southern University of Science and Technology (SUSTech), Shenzhen 518055, China.

² Hiroshima Synchrotron Radiation Center, Hiroshima University, Higashi-Hiroshima, Hiroshima 739-0046, Japan

³ School of Physics, Sun Yat-Sen University, Guangzhou 510275, China

⁴ Institute of Physics and Beijing National Laboratory for Condensed Matter Physics, Chinese Academy of Sciences, Beijing 100190, China

*These authors contributed equally to this work.

#Correspondence should be addressed to B.S. (shenbingdy@mail.sysu.edu), W.H. (huangw3@sustech.edu.cn) and C.C. (chency@sustech.edu.cn)

Abstract

The layered $\text{MnBi}_{2n}\text{Te}_{3n+1}$ family represents the first intrinsic antiferromagnetic topological insulator (AFM TI, protected by a combination symmetry S) ever discovered, providing an ideal platform to explore novel physics such as quantum anomalous Hall effect at elevated temperature and axion electrodynamics. Recent angle-resolved photoemission spectroscopy (ARPES) experiments on this family have revealed that all terminations exhibit (nearly) gapless topological surface states (TSSs) within the AFM state, violating the definition of the AFM TI, as the surfaces being studied should be S -breaking and opening a gap. Here we explain this curious paradox using a surface-bulk band hybridization picture. Combining ARPES and first-principles calculations, we prove that only an apparent gap is opened by hybridization between TSSs and bulk bands. The observed (nearly) gapless features are consistently reproduced by tight-binding simulations where TSSs are coupled to a Rashba-split bulk band. The Dirac-cone-like spectral features are actually of bulk origin, thus not sensitive to the S -breaking at the AFM surfaces. This picture explains the (nearly) gapless behaviour found in both Bi_2Te_3 - and MnBi_2Te_4 -terminated surfaces and is applicable to all terminations of $\text{MnBi}_{2n}\text{Te}_{3n+1}$ family. Our findings highlight the role of band hybridization, superior to magnetism in this case, in shaping the general surface band structure in magnetic topological materials for the first time.

Introduction:

The discovery of topological insulators (TIs) in two dimensional (2D) and three dimensional (3D) material systems has triggered a paradigm evolution in condensed matter physics, in which the phase of matter and novel properties of quantum materials are explored based on the topology of electronic structure in reciprocal space [1-3]. Combination of the electronic topology and other degrees of freedom may lead to a variety of exotic phases of matter and physical responses such as axionic excitation [4-6], Majorana state and topological superconductivity [1,7]. More specifically, the interplay between magnetism and topology could generate various quantum states, such as antiferromagnetic TI (AFM TI) [8], the quantum anomalous Hall (QAH) state [9,10] hosting dissipationless chiral edge modes [11,12], the axion insulator displaying quantized magnetoelectric effects [4-6], and the magnetic Weyl and nodal-line semimetals [13,14] which harbour Fermi arc surface states and chiral anomalies [14].

The realization of magnetic TIs [15] demands crystalline materials with both magnetic order and electronic topology. Previously, the efforts were devoted to magnetically doped TIs and magnetic topological heterostructures [11,12,16–19], whose fabrication, measurement, and property optimization are quite challenging. Recently, MnBi_2Te_4 has arisen as the first AFM TI [20-26] with periodically ordered Mn atoms on well-defined crystallographic sites, hosting possible axion electrodynamics in condensed matter. The interlayer AFM with intralayer ferromagnetic (FM) order (*c*-axis A-type AFM) occurs below a Néel temperature of about $T_N = 24.6$ K [27-34]. In particular, given a high field to fully polarize the magnetic moments, quantized Hall effect arising from Chern insulator and the transition from axion to Chern insulator have been demonstrated in MnBi_2Te_4 in the 2D limit [35-38].

Considering its topology, AFM TI MnBi_2Te_4 can be classified by a topological Z_2 invariant [8], protected by a combination symmetry $S = \Theta T_{1/2}$, where Θ is time-reversal symmetry and $T_{1/2}$ is a lattice translation symmetry of the “primitive” lattice, both broken by the AFM order but their combination preserved. At the natural cleavage (001) surface of MnBi_2Te_4 , S is broken, rendering a sizable surface state gap, which is confirmed by early angle-resolved photoemission spectroscopy (ARPES) works [20,27,32,39]. This surface gap opening is crucial to realize the half-quantum Hall effect, which may aid experimental confirmation of $\theta = \pi$ quantized magnetoelectric coupling [8]. However, subsequent systematic k_z -dependent and high-resolution ARPES measurements clearly resolved a (nearly) gapless topological surface state (TSS) Dirac cone at the (001) surface of MnBi_2Te_4 [40-43]. This gapless feature remains intact in both paramagnetic (PM) and AFM phases, and is even robust against severe surface degradation [40,44], indicating additional topological protection from magnetic, structural or electronic complication. This may explain the necessity of high field for the observation of quantized Hall effect, even in thin films with odd number of layers [37,38].

In fact, MnBi_2Te_4 belongs to the ternary van der Waals compound series $(\text{MnBi}_2\text{Te}_4)_m(\text{Bi}_2\text{Te}_3)_n$

with [Te-Bi-Te-Mn-Te-Bi-Te] septuple (S) layers ([MnBi₂Te₄], SLs) and [Te-Bi-Te-Bi-Te] quintuple (Q) layers ([Bi₂Te₃], QLs) alternately stacking along the c axis [45,46]. While MnBi₂Te₄ has been extensively studied recently [20-43], its sister compounds with higher n number such as MnBi₄Te₇ ($n = 1$) and MnBi₆Te₁₀ ($n = 2$), remain less explored [47-58]. Structurally, the FM SLs are more separated in space as n increases, reducing the interlayer AFM exchange coupling. Experimentally [48-55], MnBi₄Te₇ and MnBi₆Te₁₀ indeed show AFM transition at lower temperature (~ 13 and ~ 11 K, respectively) compared to MnBi₂Te₄. Much smaller magnetic field is needed to cause a spin flip transition. Importantly, an FM hysteresis was observed at low temperature, prerequisite for realizing the intrinsic QAH effect. However, similar to MnBi₂Te₄, controversial ARPES results exist regarding the TSSs gap in $n = 1$ and 2 compounds. For S-termination, both gapped [50,58] and gapless [48,54,56,57] TSSs have been reported. Likewise, for Q-termination (SQ-and SQQ-terminations), both gapped [48-50,57] and gapless [54-56,58] TSSs were observed, too. As all types of terminations discussed here would be S -breaking in their AFM phases, the gapless TSSs violate the definition of AFM TI for all compounds. Thus, it is of critical importance to determine the underlying mechanism of gap opening for the intrinsic surface band structure in higher n compounds.

In this work, combining ARPES, Density Functional Theory (DFT) and tight-binding (TB) analysis, we study MnBi₆Te₁₀ as an example to unveil the nature of the TSSs gap at different terminations. Using ARPES with focused Laser spot ($\sim 5 \mu\text{m}$) and superb energy and momentum resolution (μ -Laser-ARPES [59]), four types of surface-driven band structures are spatially resolved, corresponding to the three terminations of MnBi₆Te₁₀, *i.e.*, S-termination, SQ-termination, SQQ-termination and one additional SQQQ-termination resulting from either vertical stacking disorder or degradation of the topmost SLs. This assignment is well supported by the DFT slab calculations based on different surface stacking configurations. The TSSs are gapped, but not found at the Dirac point, rather in the lower Dirac cone region for S-termination and in the upper Dirac cone region for the Q-terminations. From DFT slab calculations, this gap is found to open through the hybridization of the TSSs with a bulk band. We further show, via a TB model analysis taking into account the surface-bulk hybridization, one can indeed reproduce the experimental in-gap band. In particular, within the nonmagnetic phase, a new Dirac cone overtakes the original TI Dirac cone at the Γ point for all types of terminations. These Dirac-cone-like spectral features are actually of bulk origin, thus not sensitive to the S -breaking at the surfaces of AFM phase. Our findings provide a self-consistent picture to explain the (nearly) gapless behavior of the TSSs at all intrinsic terminations of MnBi₄Te₇ and MnBi₆Te₁₀ [48,54-58], suggesting a significant role of the band hybridization in addition to other driving forces such as magnetism and spin-orbit coupling (SOC) to account for the intriguing behaviour of TSSs in the (MnBi₂Te₄) _{m} (Bi₂Te₃) _{n} family.

Results

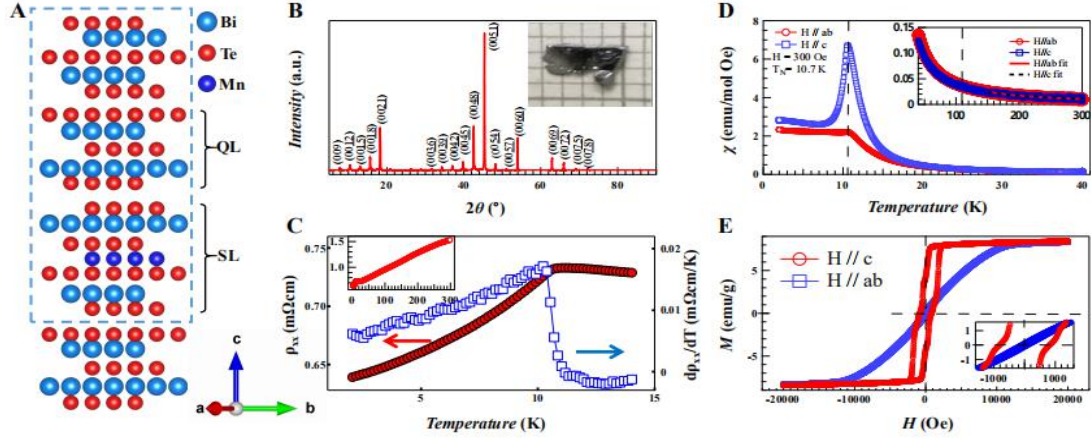


Figure 1: Lattice structure and characterization of $\text{MnBi}_6\text{Te}_{10}$ single crystals. (A), Schematic lattice structure. (B), Single crystal XRD result and peak index result. The inset shows a typical single crystal on a millimeter grid. (C), Zero-field in-plane longitudinal resistivity vs temperature. The inset shows the results up to 300 K. (D), Magnetic susceptibility vs temperature for magnetic field (300 Oe) parallel to the ab plane (red) and the c plane (blue). The inset shows the Curie–Weiss fitting for temperatures ranging from 150 K to 300 K. (E), Magnetization hysteresis at 2 K. The inset highlights the coercive fields.

$\text{MnBi}_6\text{Te}_{10}$ has a trigonal structure with a space group of $R\bar{3}m$. The lattice of $\text{MnBi}_6\text{Te}_{10}$ consists of one septuple MnBi_2Te_4 layer and two quintuple Bi_2Te_3 layers alternately stacking along the c axis (Fig. 1A). These SLs or QLs are coupled through weak van der Waals forces. Cleaving the single crystal perpendicular to the c axis could have 3 possible terminations, *i.e.*, S-termination, Q-termination and QQ-termination. The crystallinity was examined by X-ray diffraction (XRD). As shown in Fig. 1B, all peaks in the XRD pattern can be well indexed by the $(00l)$ reflections of $\text{MnBi}_6\text{Te}_{10}$.

The zero-field in-plane longitudinal resistivity $\rho_{xx}(T)$ (Fig. 1C) shows basically a monotonic decrease with decreasing temperature for $20 \text{ K} < T < 300 \text{ K}$, suggesting a metallic phase, which is confirmed by the following ARPES data. Around 10.7 K, the resistivity shows a weak upturn with decreasing temperature, likely from the enhanced electron scattering by magnetic fluctuation close to the AFM transition. On further cooling, the resistivity decreases again, indicating the gradual FM ordering of the spins in the ab plane.

The magnetic susceptibility measurement (Fig. 1D) establishes a long-range AFM order below $T_N = 10.7 \text{ K}$. A sharp cusp around T_N for $H//c$, in contrast to the saturating plateau for $H//ab$, suggests that the magnetization-easy axis is the c direction. All these behaviours are consistent with an A-type AFM configuration (intralayer FM and interlayer AFM) along c -axis. Fitting the PM regime (150 - 300 K) with the Curie–Weiss formula $\chi(T) = \chi_0 + C/(T - \theta_{CW})$ gives an

effective moment $\mu_{\text{eff}} \approx 5.4\mu_B / \text{Mn}$ and $5.1\mu_B / \text{Mn}$ for H//*c* and H//*ab*, respectively,

confirming the high spin states of Mn²⁺. The Curie–Weiss temperature is fitted as $\theta_{CW} = 9$ K and 23 K for H//*c* and H//*ab*, respectively, suggesting the existence of an additional FM interaction induced by external magnetic field. The additional FM interaction is further confirmed by the loop shape of the field-dependent magnetization [*M*(*H*)] results at 2 K (given in Fig. 1E). Compared to H//*c*, a much higher field is needed to fully polarize the spins with H//*ab*, indicating that the magnetization-easy axis is the *c*-axis. For the *c* direction, the spin-flip transition occurs at 0.2 T and the magnetic moments are fully polarized. This spin-flip field is much smaller than that in MnBi₂Te₄ (~3.5 Teslas) [29]. These features indicate that MnBi₆Te₁₀ is more suitable for exploring the intrinsic QAH effect.

All the above structural, magnetic and transport characterizations agree well with other works on the same materials [53,55]. Throughout this work, the ARPES spectra presented at the main text were measured at 20 K, meaning that the MnBi₆Te₁₀ samples stay at the PM phase. In addition, in Supplementary Section 1 we also present temperature-dependent ARPES measurements down to 6.5 K (AFM phase) for both S- and Q-terminations. No observable difference can be detected within the instrumental resolution [59].

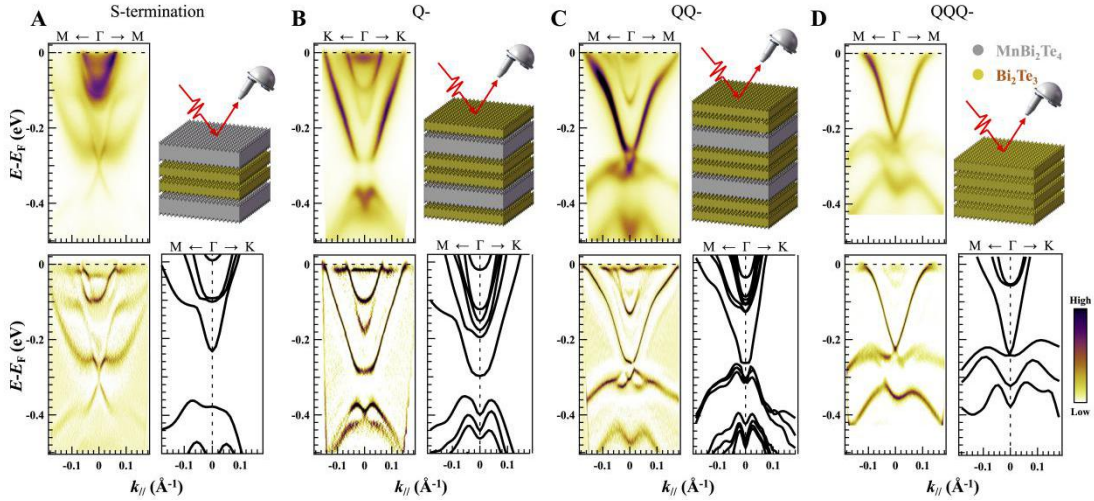


Figure 2: Termination-dependent electronic structure of MnBi₆Te₁₀ single crystals. (A, B, C, D) correspond to the results of S-, Q-, QQ- and QQQ-terminations, respectively. For each section, the top-left panel shows the raw ARPES spectra, while the bottom-left panel shows the 2nd curvature spectra. The top-right panel shows the schematic structural configuration for the corresponding DFT calculations. The bottom-right panel presents the DFT band structure, correspondingly.

To probe the intrinsic band structure of MnBi₆Te₁₀ with its different terminations, we employ a μ -Laser-ARPES system [59] with a focused laser with spot size ~ 5 μm to measure the cleaved MnBi₆Te₁₀ surface at 20 K. Figure 2 shows totally 4 types of distinct ARPES spectra which can be

distinguished from the cleaved surfaces. Also shown are the corresponding schematics of the surface termination, second-curvature spectra and the DFT band structures. The corresponding Fermi surface mapping and the dispersion along high symmetry directions are shown in Supplementary Section 1. The assignment of the measured ARPES spectra to the corresponding terminations are based on the comparison with the DFT-calculated band structure on various slab configurations (shown in the schematics). From the ARPES spectra, each termination has characteristic band dispersion. Specifically, the S-termination shows a cordial glass-shaped conduction band minimum (CBM) and gapless linear surface states with the Dirac point located at ~ 300 meV below the Fermi level (Fig. 2A). The Q-termination exhibits an apparent gap of ~ 80 meV centered at ~ 320 meV below the Fermi level and an M-shaped valence band maximum (VBM) (Fig. 2B). The band structure of QQ-termination is similar to that of Q-termination but with much smaller gap (a few meVs) (Fig. 2C). Furthermore, an additional termination with generally similar band structure to QQ-termination, but gapless TSSs and less electron doping, is resolved (Fig. 2D). Its band structure can be well reproduced by a QQQ-terminated slab. This termination likely originates from either the vertical stacking disorder or the degradation of the topmost SLs. It is worthy to note that this QQQ-termination is different from Bi_2Te_3 single crystal in the sense that, for the latter the group velocity of TSS is $\sim 3 \text{ eV}\cdot\text{\AA}$ [60] while for the former it is only $\sim 2 \text{ eV}\cdot\text{\AA}$.

Our PM ARPES spectra for S- and Q-terminations are quantitatively similar to the AFM ARPES spectra reported in Supplementary Section 1 and in Ref. [56-58]. This behaviour is consistent with previous works which prove that the TSSs show no observable change across the bulk Néel temperature within the experimental resolution in MnBi_2Te_4 [40-43]. We also calculated the total energies of several slabs with different magnetic structures (Supplementary Section 2). The total energy differences between AFM and FM states are very small (~ 2 meV/Mn), suggesting magnetic fluctuation being essential in affecting the macroscopic behavior [30-33]. This indicates that the underlying magnetic structure plays insignificant role in shaping the general band structure on the surfaces of this family of materials. These conclusions are in sharp contrast to the recent ARPES results reported in Ref. [20,22]. We note here that there are mainly three factors one need to caution in order to resolve the gapless TSSs using ARPES in this material family. The first one is micrometer-scale spatial resolution, to resolve termination-dependent band structure for $n = 1$ and $n = 2$ compounds; the second one is angular resolution, since the momentum window for the gapless features is as narrow as about $\pm 0.05 \text{ \AA}^{-1}$; the last but most important one is the tuning of the excitation photon energy, as sharp TSSs are only observable at certain low energy ranges due to the matrix element effect [40].

From Figure 2, the ARPES spectra and the DFT slab band structure show general agreement, especially for the Q-, QQ- and QQQ-terminations. However, it is their detailed discrepancies such as the gapless Dirac-cone-like features at S- and Q-terminations which DFT failed to reproduce that are puzzling researchers in this field and are the main target of our efforts in this work.

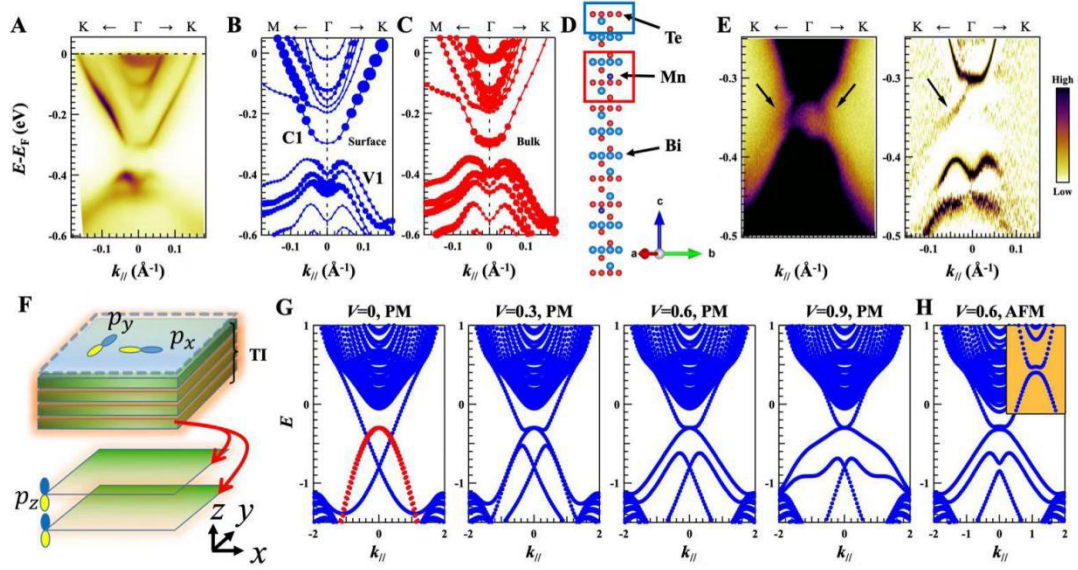


Figure 3: Surface-bulk hybridization for the Q-termination of $\text{MnBi}_6\text{Te}_{10}$. (A), the ARPES spectra of the Q-termination. (B,C,D), DFT band structure with the fatted bands projected onto corresponding layers as indicated by the blue (B) and red (C) boxes in (D). (E), Zoom in of ARPES spectra (left) and 2nd curvature (right) to highlight the in-gap states. (F), Schematic of the TB model. (G), TB simulated results and the band structure evolution with increasing hybridization at the PM state. The red curves represent the original RSB bands. (H), TB simulated bands with AFM order. The insets highlight the CBM splitting.

Figure 3A-E highlight the discrepancy between the experimental ARPES spectra and the DFT slab simulation for the Q-termination. Since general agreement has been reached between ARPES and DFT concerning the shape of CBM and VBM, and the gap size between them (Fig. 3A-C), experimentally the emergence of one in-gap band (indicated by black arrows in Fig. 3E), which DFT fails to reproduce, is quite unusual. The cusp of this in-gap band touches the CBM, forming a gapless Dirac-cone-like feature. Similar results have been reported by other groups at the Q-terminations in MnBi_4Te_7 [54,56] and $\text{MnBi}_6\text{Te}_{10}$ [56,58].

We firstly try to track down the origin of the apparent gap. As shown by the DFT calculated bands and the corresponding projection to different layers in Fig. 3B-D, the lowest conduction band (C1) is mainly surface-originated, with surface domination increasing with the wave vector. At the Γ point, however, C1 is dominated by bulk states. For the highest valence band (V1), the opposite occurs. The surface states dominate around Γ and bulk contribution increases with wave vector. This demonstrates a surface-bulk band hybridization and gap opening due to the “avoided crossing” [61]. We then proceed to use a tight binding (TB) model analysis to show that this hybridization can indeed lead to the emergence of the apparent gap and the additional in-gap states (Fig. 3E).

For simplicity, we consider a scenario where the TSS Dirac cone hybridize with additional quasi-two-dimensional Rashba-split bulk bands (RSB). These RSBs are not intrinsically related to the underlying topological insulating phase. They originate from bulk bands which gain surface

characteristic due to their proximity to the surface, similar to the quantum well states observed at the surfaces of typical TI Bi_2Se_3 family [44]. Traces of this identification can indeed be found in the DFT calculations (Fig. 3B and C). As schematically drawn in Fig. 3F, the TI is modeled by a 3D stacking of bilayers of p_z -like Wannier orbitals, which has been shown to be appropriate for this series of TIs [24]. The RSBs may originate from either certain additional p_z orbitals, or certain p_x/p_y -like Wannier orbitals which lie close in energy. In our simplified model, we consider spin-orbit coupled $(p_x + ip_y) \uparrow$ and $(p_x - ip_y) \downarrow$ Wannier orbitals in a fictitious layer. Note that they are the only p -wave states that could be distinguished from the TI p_z -orbitals under the C_3 symmetry at the surface of the TI. Nevertheless, the results are qualitative similar if the RSBs come from p_z -like orbitals instead, as we shall mention later. The RSB orbitals couple with the topmost bilayer of the TI, and the effective Hamiltonian reads,

$$H = H_{TI} + H_{RSB} + H_{hyb}.$$

In order, the three terms stand for the Hamiltonian of the TI, the RSBs, and the hybridization. While more details are provided in the Supplementary Section 3, the hybridization term deserves a special attention. Expanded around the Γ -point, it reads,

$$H_{hyb} = V \sum_{m,k} (-1)^m [(k_x - ik_y) c_{0m\uparrow}^\dagger d_{k\uparrow} + (k_x + ik_y) c_{0m\downarrow}^\dagger d_{k\downarrow}] + \text{H.c.},$$

where, V denotes the strength of the hybridization, c_{0m}^\dagger and c_{0m} represent the creation and annihilation of p_z -orbitals on the top TI bilayer where $m = 0,1$ index its two sublayers, and, $d_{\uparrow(\downarrow)}^\dagger$ and $d_{\uparrow(\downarrow)}$ create and annihilate the respective $(p_x + ip_y) \uparrow$ and $(p_x - ip_y) \downarrow$ orbitals of the RSBs. It is important to note that the time-reversal and C_3 symmetry ensures that the hybridization vanishes at the Γ point, meaning that the Dirac crossings of the RSBs and that of the TSSs remain intact. Due to the finite hybridization away from the Γ point, the two Dirac crossings switch designations, *i.e.*, the original RSB crossing become the crossing of the new Dirac cone that connects the conduction and valence bands, and vice versa. In this manner, the essential topological properties of the hybrid system are unaltered from the original TI. As a side remark, had we considered RSBs originating from other orbitals, such as one with p_z -symmetry, the hybridization between the two Dirac crossings at the Γ point becomes finite, shifting their relative energy. However, this hybridization does not lift the degeneracy of the individual crossings so long as time reversal symmetry is preserved. Hence, as in the above case, the two crossings switch designations and the overall topology remains.

In Fig. 3G, we present the results of typical TB simulations of the Q-termination within the PM state, in which only the hybridization strength V is varied. Note that in this case a small Rashba SOC is taken for the RSBs in order to obtain a good fit. For $V = 0$, the TSSs (blue) and RSBs (red) remain intact. With increasing V , the main features of the experimental spectra are readily reproduced, including the M-shaped VBM, the hybridization gap and the hole-type in-gap states.

Further inclusion of AFM order (Fig. 3H) can even reproduce the small gap in the original Dirac cone observed by ARPES here (Fig. 3E), and the tiny splitting at the CBM, which is observed by others [58].

Within this picture, those intriguing features found in the experimental spectra of Q-terminations (Fig. 3E) can now be understood. The M-shaped VBM consists of the original TSS Dirac cone and RSBs; the apparent gap opens in the upper Dirac cone region due to the surface-bulk hybridization; the gapless feature comes from the symmetry-protected touching of the gapped TSSs and split RSBs at the Γ point. With AFM order, gaps are opened at both original TSS Dirac cone and the new touching point, but the gap size could be so small that extrinsic factors can smear it easily.

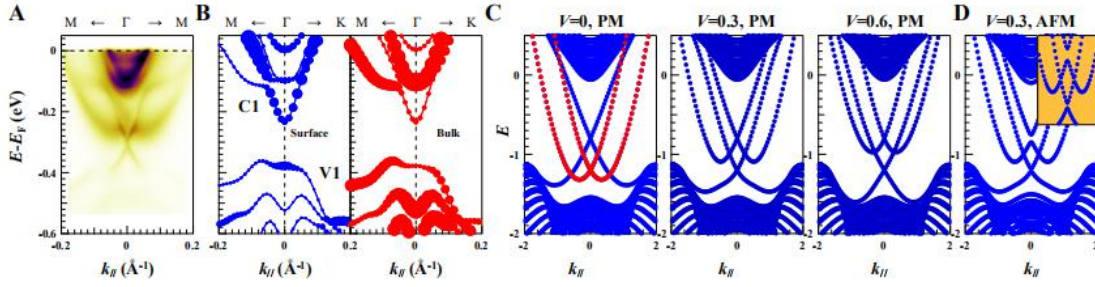


Figure 4: Surface-bulk hybridization for the S-termination of MnBi₆Te₁₀. (A), the ARPES spectra. (B), DFT band structure with the fatted bands projected onto corresponding surface (blue filled circles) and bulk layers (red filled circles). (C), TB model simulated band structure and its evolution with increasing hybridization at PM state. The red curves represent the original RSB bands. (D), TB simulated bands at AFM order. The inset highlights the tiny gap of the new TSSs.

This TB hybridization model is also applicable to the band structure of S-termination shown in Fig. 4. Similarly, from DFT, the C1 band is surface-dominated and V1 is bulk-dominated while around the Γ point the opposite happens, suggesting a surface-bulk hybridization picture (Fig. 4B). In Fig. 4C, we use the TB model presented above to model the S-termination bands. This time CBM-like RSBs hybridize with the lower Dirac cone of TSSs. With appropriate SOC and increasing V , the cordial glass-shaped CBM and gapless linear Dirac cones start to manifest. The $V = 0.3$ panel matches the experimental spectra the most. In Fig. 4D, the AFM order is included in the simulation and tiny gaps opens in the new Dirac cone, in agreement with ARPES results [58]. The consequent (nearly) gapless features at S-termination thus come from the original RSB Dirac cone. The original TSS Dirac cone gains broadness due to its hybridization with bulk states and its tiny gap at AFM state is smeared.

We have demonstrated the applicability of a surface-bulk hybridization model to account for the band structure at the S- and Q-terminations of MnBi₆Te₁₀. Built on the DFT orbital projection analyses, this model is well-grounded and provides a unique physical picture to explain the (nearly) gapless behaviour of TSSs for all terminations. In this picture, the Dirac cones identified by ARPES are of bulk origin, with wave functions extending much more deeply into the crystal than the non-hybridized ones. This means that the impact of S symmetry breaking at the surface on

these spectral features is dramatically reduced, naturally explaining their (nearly) gapless behaviour at all surfaces within AFM phase. Due to their similarity in the lattice structure and band structure, the universal (nearly) gapless behaviour from all terminations of $(\text{MnBi}_2\text{Te}_4)_m(\text{Bi}_2\text{Te}_3)_n$ can be understood now in this picture.

MATERIALS AND METHODS

Sample growth and characterization

High quality $\text{MnBi}_6\text{Te}_{10}$ single crystals were grown by the conventional high-temperature solution method with Bi_2Te_3 as the flux. Mn (purity 99.98%), Bi (purity 99.999%) and Te (99.999%) blocks were placed in an alumina crucible with a molar ratio of Mn: Bi: Te = 1: 11.3: 18. Then the alumina crucible was sealed in a quartz tube under the argon environment. The assembly was first heated up in a box furnace to 950°C , held for 10 hrs, then subsequently cooled down to 700°C over 10 hrs and further cooled down slowly to 575°C over 100 hrs. After this heating procedure, the quartz tube was taken out quickly and then decanted into the centrifuge to remove the excess flux from the single crystals.

Resistivity measurement were performed by a Quantum Design (QD) Physical Properties Measurement System (PPMS) with a standard six-probe method. The driven current is 10 mA and flows in the *ab* plane. Magnetic measurements were performed using the QD PPMS with the Vibrating Sample Magnetometer (VSM) mode. Temperature dependent magnetization results were collected with an external magnetic field of 300 Oe, both along and perpendicular to the *c*-axis direction of the sample.

ARPES measurement

μ -Laser-ARPES measurements were performed at the Hiroshima Synchrotron Radiation Center (HSRC), Hiroshima, Japan with a VG Scienta R4000 electron analyzer and a photon energy of 6.3 eV [59]. The energy and angular resolution were better than 3 meV and less than 0.05° , respectively. Samples were cleaved *in situ* along the (001) crystal plane under ultra-high vacuum conditions with pressure better than 5×10^{-11} mbar and temperatures below 25 K.

DFT Calculation method

First-principles calculations were performed using the Vienna *ab initio* simulation package (VASP) [62,63] within the framework of density-functional theory [64,65]. The generalized gradient approximation (GGA) with the Perdew-Burke-Ernzerhof (PBE) formalism was chosen for the exchange-correlation functional [66]. The projector augmented wave (PAW) method was implemented to treat core-valence interactions with a cutoff energy of 400 eV for the plane-wave expansion [67,68]. The full Brillouin zone was sampled by a $8 \times 8 \times 1$ Monkhorst-Pack grid [69]. The slab structures (including both lattice and fractional coordinates) were fully relaxed until the forces on each atom were less than $0.01 \text{ eV}/\text{\AA}$. Considering the strongly correlated nature of $3d$ electrons in Mn, we introduced on-site Coulomb repulsion by employing GGA+U calculations [70] and set the correlation energy to be 5 eV, which worked well in the previous works [71].

Tight binding simulation method

We construct a model to effectively simulate the hybridization between the TI surface states and a pair of Rashba-split bulk bands. Since we are only concerned about the physics around the Γ -point, it suffices to build the model on a lattice with tetragonal symmetry to keep the expressions in their simplest forms. No essential feature of the hybridization in question is lost due to this simplification. We generalize a standard $k\cdot p$ theory of TI [72] to a 3D lattice model, which is formed by a stacking of bilayers with each sublayer featuring a p_z -orbital. Regarding the hybridization to bulk states, we consider that the topmost bilayer of the TI is coupled to an extra band with Rashba SOC, whose band top (or bottom) overlaps with the TSSs in momentum space. More details can be found in the Supplementary Section 3.

ACKNOWLEDGEMENTS

We thank Qihang Liu, Junhao Lin, Liusuo Wu, Weiqiang Chen and Haizhou Lu for helpful discussions. J.F.S is supported by the National Foundation for Young Scientists of China (Grant No. 11804402). C.L. is supported by the National Natural Science Foundation of China (NSFC) (No. 11504159 and No. 11674149), NSFC Guangdong (No. 2016A030313650), the Guangdong Innovative and Entrepreneurial Research Team Program (No. 2016ZT06D348), the Shenzhen Key Laboratory (Grant No. ZDSYS20170303165926217), and the Technology and Innovation Commission of Shenzhen Municipality (Grants No. JCYJ20150630145302240 and No. KYTDPT 20181011104202253). X.J.Z is supported by the National Key Research and Development Program of China (Grant No. 2016YFA0300300 and 2017YFA0302900) and the National Natural Science Foundation of China (Grant No. 11888101). H.X. is supported by Center for Computational Science and Engineering at Southern University of Science and Technology. B.S. is supported by the Hundreds of Talents program of Sun Yat-Sen University, the Fundamental Research Funds for the Central Universities. W.H. thank the startup grant at SUSTech. The ARPES measurements were performed with the approval of the Proposal Assessing Committee of the Hiroshima Synchrotron Radiation Center (Proposal Numbers: 19AU002, 19AU007 & 19BG006).

References:

1. Xiaoliang Qi and Shoucheng Zhang, Topological insulators and superconductors. *Rev. Mod. Phys.* **83**, 1057 (2011).
2. M. Z. Hasan and C.L. Kane, Colloquium: Topological insulators. *Rev. Mod. Phys.* **82**, 3045 (2010).
3. Yoichi Ando and Liang Fu, Topological crystalline insulators and topological superconductors: From concepts to materials. *Annu. Rev. Condens. Matter Phys.* **6**, 361 (2015).
4. N. P. Armitage and Liang Wu, On the matter of topological insulators as magnetoelectrics. *Sci. Post. Phys.* **6**, 046 (2019).
5. Di Xiao, Jue Jiang, Jae-Ho Shin, Wenbo Wang, Fei Wang, Yi-Fan Zhao, Chaoxiong Liu, Weida Wu, Moses H. W. Chan, Nitin Samarth and Cui-Zu Chang, Realization of the axion insulator state in quantum anomalous hall sandwich heterostructures. *Phys. Rev. Lett.* **120**, 056801 (2018).
6. Jing Wang, Biao Lian, Xiao-Liang Qi and Shou-Cheng Zhang, Quantized topological magnetoelectric effect of the zero-plateau quantum anomalous Hall state. *Phys. Rev. B* **92**, 081107 (2015).
7. Liang Fu and C. L. Kane, Superconducting proximity effect and Majorana fermions at the surface of a topological insulator. *Phys. Rev. Lett.* **100**, 096407 (2008).
8. Rongter S. K. Mong, Andrew M. Essin and Joel E. Moore, Antiferromagnetic topological insulators. *Phys. Rev. B* **81**, 245209 (2010).
9. F. D. M. Haldane, Model for a quantum Hall effect without Landau levels: Condensed matter realization of the parity anomaly. *Phys. Rev. Lett.* **61**, 2015 (1988).
10. Rui Yu, Wei Zhang, Hai-Jun Zhang, Shou-Cheng Zhang, Xi Dai and Zhong Fang, Quantized anomalous Hall effect in magnetic topological insulators. *Science* **329**, 61 (2010).
11. Cui-Zu Chang, Jinsong Zhang, Xiao Feng, Jie Shen, Zuocheng Zhang, Minghua Guo, Kang Li, Yunbo Ou, Pang Wei, Li-Li Wang, Zhong-Qing Ji, Yang Feng, Shuaihua Ji, Xi Chen, Jingfeng Jia, Xi Dai, Zhong Fang, Shou-Cheng Zhang, Ke He, Yayu Wang, Li Lu, Xu-Cun Ma, Qi-Kun Xue, Experimental observation of the quantum anomalous Hall effect in a magnetic topological insulator. *Science* **340**, 167 (2013).
12. Cui-Zu Chang, Weiwei Zhao, Duk Y. Kim, Haijun Zhang, Badih A. Assaf, Don Heiman, Shou-Cheng Zhang, Chaoxing Liu, Moses H. W. Chan, Jagadeesh S. Moodera, High-precision realization of robust quantum anomalous Hall state in a hard ferromagnetic topological insulator. *Nat. Mater.* **14**, 473 (2015).
13. Kyoo Kim, Junho Seo, Eunwoo Lee, K.-T. Ko, B. S. Kim, Bo Gyu Jang, Jong Mok Ok,

- Jinwon Lee, Youn Jung Jo, Woun Kang, Ji Hoon Shim, C. Kim, Han Woong Yeom, Byung Il Min, Bohm-Jung Yang and Jun Sung Kim, Large anomalous Hall current induced by topological nodal lines in a ferromagnetic van der Waals semimetal. *Nat. Mater.* **17**, 794 (2018).
14. N. P. Armitage, E. J. Mele, Ashvin Vishwanath, Weyl and Dirac semimetals in three-dimensional solids. *Rev. Mod. Phys.* **90**, 015001 (2018).
 15. Yoshinori Tokura, Kenji Yasuda and Atsushi Tzukazaki, Magnetic topological insulators. *Nature Rev. Phys.* **1**, 126 (2019).
 16. Ferhat Katmis, Valeria Lauter, Flavio S. Nogueira, Badih A. Assaf, Michelle E. Jamer, Peng Wei, Biswarup Satpati, John W. Freeland, Ilya Eremin, Don Heiman, Pablo Jarillo-Herrero and Jagadeesh S. Moodera, A high-temperature ferromagnetic topological insulating phase by proximity coupling. *Nature* **533**, 513 (2016).
 17. M. Mogi, M. Kawamura, R. Yoshimi, A. Tsukazaki, Y. Kozuka, N. Shirakawa, K. S. Takahashi, M. Kawasaki and Y. Tokura, A magnetic heterostructure of topological insulators as a candidate for an axion insulator. *Nat. Mater.* **16**, 516 (2017).
 18. M M Otrokov, T V Menshchikova, M G Vergniory, I P Rusinov, A Yu Vyazovskaya, Yu M Koroteev, G Bihlmayer, A Ernst, P M Echenique, A Arnau and E V Chulkov, Highly-ordered wide bandgap materials for quantized anomalous Hall and magnetoelectric effects. *2D Mater.* **4**, 025082 (2017).
 19. M. M. Otrokov, T. V. Menshchikova, I. P. Rusinov, M. G. Vergniory, V. M. Kuznetsov and E. V. Chulkov, Magnetic extension as an efficient method for realizing the quantum anomalous hall state in topological insulators. *JETP Lett.* **105**, 297 (2017).
 20. M. M. Otrokov, I. I. Klimovskikh, H. Bentmann, D. Estyunin, A. Zeugner, Z. S. Aliev, S. Gaß, A. U. B. Wolter, A. V. Koroleva, A. M. Shikin, M. Blanco-Rey, M. Hoffmann, I. P. Rusinov, A. Yu. Vyazovskaya, S. V. Ereemeev, Yu. M. Koroteev, V. M. Kuznetsov, F. Freyse, J. Sánchez-Barriga, I. R. Amiraslanov, M. B. Babanly, N. T. Mamedov, N. A. Abdullayev, V. N. Zverev, A. Alfonsov, V. Kataev, B. Büchner, E. F. Schwier, S. Kumar, A. Kimura, L. Petaccia, G. Di Santo, R. C. VIDA, S. Schatz, K. Kißner, M. Ünzelmann, C. H. Min, Simon Moser, T. R. F. Peixoto, F. Reinert, A. Ernst, P. M. Echenique, A. Isaeva and E. V. Chulkov, Prediction and observation of an antiferromagnetic topological insulator. *Nature* **576**, 416 (2019).
 21. Roger S. K. Mong and Koel E. Moore, Magnetic and topological order united in a crystal. *Nature* **576**, 390 (2019).
 22. E. D. L. Rienks, S. Wimmer, J. Sánchez-Barriga, O. Caha, P. S. Mandal, J. Rrmůžička, A. Ney, H. Steiner, V. V. Volobuev, H. Groiss, M. Albu, G. Kothleitner, J. Michalička, S. A. Khan, J. Minár, H. Ebert, G. Bauer, F. Freyse, A. Varykhalov, O. Rader and G. Springholz, Large magnetic map at the Dirac point in $\text{Bi}_2\text{Te}_3/\text{MnBi}_2\text{Te}_4$ heterostructures. *Nature* **576**, 423 (2019).

23. M. M. Otrokov, I. P. Rusinov, M. Blanco-Rey, M. Hoffmann, A. Yu. Vyazovskaya, S. V. Eremeev, A. Ernst, P. M. Echenique, A. Arnau and E. V. Chulkov, Unique thickness-dependent properties of the van der Waals interlayer antiferromagnet MnBi_2Te_4 films. *Phys. Rev. Lett.* **122**, 107202 (2019).
24. Jiaheng Li, Yang Li, Shiqiao Du, Zun Wang, Bing-Lin Gu, Shou-Cheng Zhang, Ke He, Wen-hui Duan and Yong Xu, Intrinsic magnetic topological insulators in van der Waals layered MnBi_2Te_4 -family materials. *Sci. Adv.* **5**, eaaw5685 (2019).
25. Jiaheng Li, Chong Wang, Zetao Zhang, Bing-Lin Gu, Wenhui Duan and Yong Xu, Magnetically controllable topological quantum phase transitions in the antiferromagnetic topological insulator MnBi_2Te_4 . *Phys. Rev. B* **100**, 121103(R) (2019).
26. Dongqin Zhang, Minji Shi, Tongshuai Zhu, Dingyu Xing, Haijun Zhang and Jing Wang, Topological axion states in the magnetic insulator MnBi_2Te_4 with the quantized magnetoelectric effect. *Phys. Rev. Lett.* **122**, 206401 (2019).
27. Alexander Zeugner, Frederik Nietschke, Anja U. B. Wolter, Sebastian Gaß, Raphael C. Vidal, Thiago R. F. Peixoto, Darius Pohl, Christine Damm, Axel Lubk, Richard Hentrich, Simon K. Moser, Celso Fornari, Chul Hee Min, Sonja Schatz, Katharina Kißner, Maximilian Ünzelmann, Martin Kaiser, Francesco Scaravaggi, Bernd Rellinghaus, Kornelius Nielsch, Christian Hess, Bernd Büchner, Friedrich Reinert, Hendrik Bentmann, Oliver Oeckler, Thomas Doert, Michael Ruck and Anna Isaeva, Chemical aspects of the candidate antiferromagnetic topological insulator MnBi_2Te_4 . *Chem. Mater.* **31**, 2795 (2019).
28. Jianhua Cui, Mengzhu Shi, Honghui Wang, Fanghang Yu, Tao Wu, Xigang Luo, Janjun Ying and Xianhui Chen, Transport properties of thin flakes of the antiferromagnetic topological insulator MnBi_2Te_4 . *Phys. Rev. B* **99**, 155125 (2019).
29. J.-Q. Yan, Q. Zhang, T. Heitmann, Zengle Huang, K. Y. Chen, J.-G. Cheng, Weida Wu, D. Vaknin, B. C. Sales and R. J. McQueeney, Crystal growth and magnetic structure of MnBi_2Te_4 . *Phys. Rev. Mat.* **3**, 064202 (2019).
30. J.-Q. Yan, S. Okamoto, M. A. McGuire, A. F. May, R. J. McQueeney and B. C. Sales, Evolution of structural, magnetic, and transport properties in $\text{MnBi}_{2-x}\text{Sb}_x\text{Te}_4$. *Phys. Rev. B* **100**, 104409 (2019).
31. J.-Q. Yan, D. Pajeroski, Liqin Ke, A.-M. Nedić, Y. Sizyuk, Elijah Gordon, P. P. Orth, D. Vaknin and R. J. McQueeney, Competing magnetic interactions in the antiferromagnetic topological insulator MnBi_2Te_4 . arXiv:1908.02332 (2019).
32. Seng Huat Lee, Yanglin Zhu, Yu Wang, Leixin Miao, Timothy Pillsbury, Hemian Yi, Susan Kempinger, Jin Hu, Colin A. Heikes, P. Quarterman, William Ratchliff, Julie A. Borchers, Heda Zhang, Xianglin Ke, David Graf, Nasim Alem, Cui-Zu Chang, Nitin Samarth and Zhiqiang Mao, Spin scattering and noncollinear spin structure-induced intrinsic anomalous Hall effect in antiferromagnetic topological insulator MnBi_2Te_4 . *Phys. Rev. Research* **1**,

012011(R) (2019).

33. K. Y. Chen, B. S. Wang, J.-Q. Yan, D. S. Parker, J.-S. Zhou, Y. Uwatoko and J.-G. Cheng, Suppression of the antiferromagnetic metallic state in the pressurized MnBi_2Te_4 single crystal. *Phys. Rev. Materials* **3**, 094201 (2019).
34. Hao Li, Shengsheng Liu, Chang Liu, Jingsong Zhang, Yong Xu, Rong Yu, Yang Wu, Yuegang Zhang and Shoushan Fan, Antiferromagnetic topological insulator MnBi_2Te_4 : Synthesis and magnetic properties. *Phys. Chem. Chem. Phys.* (DOI: 10.1039/C9CP05634C) (2019).
35. Yan Gong, Jingwen Guo, Jiaheng Li, Kejing Zhu, Menghan Liao, Xiaozhi Liu, Qinghua Zhang, Lin Gu, Lin Tang, Xiao Feng, Ding Zhang, Wei Li, Canli Song, Lili Wang, Pu Yu, Xi Chen, Yayu Wang, Hong Yao, Wenhui Duan, Yong Xu, Shou-Cheng Zhang, Xucun Ma, Qi-Kun Xue and Ke He, Experimental realization of an intrinsic magnetic topological insulator. *Chin. Phys. Lett.* **36**, 076801 (2019).
36. Chang Liu, Yongchao Wang, Hao Li, Yang Wu, Yaoxin Li, Jiaheng Li, Ke He, Yong Xu, Jinsong Zhang and Yayu Wang, Quantum phase transition from axion insulator to Chern insulator in MnBi_2Te_4 . arXiv:1905.00715 (2019).
37. Yujun Deng, Yijun Yu, Meng Zhu Shi, Jing Wang, Xian Hui Chen and Yuanbo Zhang, Magnetic-field-induced quantized anomalous Hall effect in intrinsic magnetic topological insulator MnBi_2Te_4 . arXiv:1904.11468 (2019).
38. Jun Ge, Yanzhao Liu, Jiaheng Li, Hao Li, Tianchuang Luo, Yang Wu, Yong Xu and Jian Wang, High- Chern-number and high-temperature quantum Hall effect without Landau levels. arXiv:1907.09947 (2019).
39. R. C. Vidal, H. Bentmann, T. R. F. Peixoto, A. Zeugner, S. Moser, C.-H. Min, S. Schatz, K. Kißner, M. Ünzelmann, C. I. Fornari, H. B. Vasili, M. Valvidares, K. Sakamoto, D. Mondal, J. Fujii, I. Vobornik, S. Jung, C. Cacho, T. K. Kim, R. J. Koch, C. Jozwiak, A. Bostwick, J. D. Denlinger, E. Rotenberg, J. Buck, M. Hoesch, F. Diekmann, S. Rohlf, M. Källäne, K. Rossnagel, M. M. Otrokov, E. V. Chulkov, M. Ruck, A. Isaeva and F. Reinert, Surface states and Rashba-type spin polarization in antiferromagnetic MnBi_2Te_4 (0001). *Phys. Rev. B* **100**, 121104(R) (2019).
40. Yu-Jie Hao, Pengfei Liu, Yue Feng, Xiao-Ming Ma, Eike F. Schwier, Masashi Arita, Shiv Kumar, Chaowei Hu, Ruie Lu, Meng Zeng, Yuan Wang, Zhanyang Hao, Hong-Yi Sun, Ke Zhang, Jiawei Mei, Ni Ni, Liusuo Wu, Kenya Shimada, Chaoyu Chen, Qihang Liu and Chang Liu, Gapless surface Dirac cone in antiferromagnetic topological insulator MnBi_2Te_4 . *Phys. Rev. X* **9**, 041038 (2019).
41. Hang Li, Shun-Ye Gao, Shao-Feng Duan, Yuan-Feng Xu, Ke-Jia Zhu, Shang-Jie Tian, Jia-Cheng Gao, Wen-Hui Fan, Zhi-Cheng Rao, Jie-Rui Huang, Jia-Jun Li, Da-Yu Yan, Zheng-Tai Liu, Wan-Ling Liu, Yao-Bo Huang, Yu-Liang Li, Yi Liu, Guo-Bin Zhang, Peng

- Zhang, Takeshi Kondo, Shik Shin, He-Chang Lei, You-Guo Shi, Wen-Tao Zhang, Hong-MingWeng, Tian Qian and Hong Ding, Dirac surface states in intrinsic magnetic topological insulators EuSn_2As_2 and $\text{MnBi}_{2n}\text{Te}_{3n+1}$. *Phys. Rev. X* **9**, 041039 (2019).
42. Y. J. Chen, L. X. Xu, J. H. Li, Y. W. Li, H. Y. Wang, C. F. Zhang, H. Li, Y. Wu, A. J. Liang, C. Chen, S. W. Jung, C. Cacho, Y. H. Mao, S. Liu, M. X. Wang, Y. F. Guo, Y. Xu, Z. K. Liu, L. X. Yang and Y. L. Chen, Topological electronic structure and its temperature evolution in antiferromagnetic topological insulator MnBi_2Te_4 . *Phys. Rev. X* **9**, 041040, (2019).
 43. Przemyslaw Swatek, Yun Wu, Lin-Lin Wang, Kyungchan Lee, Benjamin Schruck, Jiaqiang Yan and Adam Kaminski, Gapless Dirac surface states in the antiferromagnetic topological insulator MnBi_2Te_4 . arXiv:1907.09596 (2019).
 44. Chaoyu Chena, Shaolong Hea, Hongming Wenga, Wentao Zhanga, Lin Zhaoa, Haiyun Liua, Xiaowen Jiaa, Daixiang Moua, Shanyu Liua, Junfeng Hea, Yingying Penga, Ya Fenga, Zhuojin Xiea, Guodong Liua, Xiaoli Donga, Jun Zhanga, Xiaoyang Wangb, Qinjun Pengb, Zhimin Wangb, Shenjin Zhangb, Feng Yangb, Chuangtian Chenb, Zuyan Xub, Xi Daia, Zhong Fanga, and X. J. Zhou, Robustness of topological order and formation of quantum well states in topological insulators exposed to ambient environment. *Proc. Natl. Acad. Sci. USA* **109**, 3694 (2012).
 45. Ziya S. Aliev, Imamaddin R. Amirasanov b, Daria I. Nasonova c, Andrei V. Shevelkov c, Nadir A. Abdullayev b, Zakir A. Jahangirli b, Elnur N. Orujlu d, Mikhail M. Otrokov, Nazim T. Mamedov b, Mahammad B. Babanly d and Evgueni V. Chulkov, Novel ternary layered manganese bismuth tellurides of the $\text{MnTe-Bi}_2\text{Te}_3$ system: Synthesis and crystal structure. *J. Alloy. Comp.* **789**, 443 (2019).
 46. Daniel Souchay, Markus Nentwig, Daniel Günther, Simon Keilholz, Johannes de Boor, Alexander Zeugner, Anna Isaeva, Michael Ruck, Anja U. B. Wolter, Bernd Büchner and Oliver Oeckler, Layered manganese bismuth tellurides with GeBi_4Te_7 - and $\text{GeBi}_6\text{Te}_{10}$ -type structures: towards multifunctional materials. *J. of Mater. Chem. C* **7**, 9939 (2019).
 47. Hongyi Sun, Bowen Xia, Zhongjia Chen, Yingjie Zhang, Pengfei Liu, Qiushi Yao, Hong Tang, Yujun Zhao Hu Xu and Qihang Liu, Rational design principle of the quantum anomalous Hall effect in superlatticelike magnetic topological insulators. *Phys. Rev. Lett.* **123**, 096401(2019).
 48. Chaowei Hu, Kyle N. Gordon, Pengfei Liu, Jinyu Liu, Xiaoqing Zhou, Peipei Hao, Dushyant Narayan, Eve Emmanouilidou, Hongyi Sun, Yuntian Liu, Harlan Brawer, Arthur P. Ramirez, Lei Ding, Huibo Cao, Qihang Liu, Dan Dessau and Ni Ni, A van der Waals antiferromagnetic topological insulator with weak interlayer magnetic coupling. arXiv:1905.02154 (2019).
 49. Jiazhen Wu, Fucai Liu, Masato Sasase, Koichiro Inaga, Yukiko Obata, Ryu Yukawa, Koji Horiba, Hiroshi Kumigashira, Satoshi Okuma, Takeshi Inoshita, Hideo Hosono, Natural van der Waals heterostructures with tunable magnetic and topological states. *Sci. Adv.* **5**,

eaax9989 (2019).

50. Raphael C. Vidal, Alexander Zeugner, Jorge I. Facio, Rajyavardhan Ray, M. Hossein Haghghi, Anja U. B. Wolter, Laura T. Corredor Bohorquez, Federico Cagliaris, Simon Moser, Tim Figgemeier, Thiago R. F. Peixoto, Hari Babu Vasili, Manuel Valvidares, Sungwon Jung, Cephise Cacho, Alexey Alfonsov, Kavita Mehlawat, Vladislav Kataev, Christian Hess, Manuel Richter, Bernd Bchner, Jeroen van den Brink, Michael Ruck, Friedrich Reinert, Hendrik Bentmann, Anna Isaeva Topological electronic structure and intrinsic magnetization in MnBi_4Te_7 : a Bi_2Te_3 -derivative with a periodic Mn sublattice. arXiv:1906.08394.
51. J.-Q. Yan, Y. H. L., D. Parker, M. A. McGuire, B. C. Sales. A-type Antiferromagnetic order in MnBi_4Te_7 and $\text{MnBi}_6\text{Te}_{10}$ single crystals. arXiv:1910.06273 (2019).
52. Lei Ding, Chaowei Hu, Feng Ye, Erxi Feng, Ni Ni and Huibo Cao. Crystal and magnetic structure of magnetic topological insulators $\text{MnBi}_{2n}\text{Te}_{3n+1}$. arXiv:1910.06248 (2019).
53. M. Z. Shi, B. L., C. S. Zhu, D. H. Ma, J. H. Cui, Z. L. Sun, J. J. Ying and X. H. Chen. Magnetic and transport properties in the magnetic topological insulators $\text{MnBi}_2\text{Te}_4(\text{Bi}_2\text{Te}_3)_n$ ($n = 1,2$). Phys. Rev. B **100** 155144 (2019).
54. L. X. Xu, Y. H. M., H. Y. Wang, J. H. Li, Y. J. Chen, Y. Y. Y. Xia, Y. W. Li, J. Zhang, H. J. Zheng, K. Huang, C. F. Zhang, S. T. Cui, A. J. Liang, W. Xia, H. Su, S. W. Jung, C. Cacho, M. X. Wang, G. Li, Y. Xu, Y. F. Guo, L. X. Yang, Z. K. Liu, Y. L. Chen. Persistent gapless surface states in $\text{MnBi}_2\text{Te}_4/\text{Bi}_2\text{Te}_3$ superlattice antiferromagnetic topological insulator. arXiv:1910.11014 (2019).
55. Shangjie Tian, Shunye Gao, Simin Nie, Yuting Qian, Chunsheng Gong, Yang Fu, Hang Li, Wenhui Fan, Peng Zhang, Takesh Kondo, Shik Shin, Johan Adell, Hanna Fedderwitz, Hong Ding, Zhijun Wang, Tian Qian and Hechang Lei. Magnetic topological insulator in $\text{MnBi}_6\text{Te}_{10}$ with zero-field ferromagnetic state. arXiv:1910.10101 (2019).
56. Yong Hu, L. X., Mengzhu Shi, Aiyun Luo, Shuting Peng, Z.Y.Wang, J.J.Ying, T.Wu, Z.K.Liu, C.F.Zhang, Y.L.Chen, G.Xu, X.-H.Chen, J.-F.He. Universal gapless Dirac cone and tunable topological states in $(\text{MnBi}_2\text{Te}_4)_m(\text{Bi}_2\text{Te}_3)_n$ heterostructures. arXiv:1910.11323 (2019).
57. Kyle N. Gordon, H. S., Chaowei Hu, A. Garrison Linn, Haoxiang Li, Yuntian Liu, Pengfei Liu, Scott Mackey, Qihang Liu, Ni Ni, Dan Dessau. Strongly gapped topological surface states on protected surfaces of antiferromagnetic MnBi_4Te_7 and $\text{MnBi}_6\text{Te}_{10}$. arXiv:1910.13943 (2019).
58. Na Hyun Jo, Lin-Lin Wang, Robert-Jan Slager, Jiaqiang Yan, Yun Wu, Kyungchan Lee, Benjamin Schruck, Ashvin Vishwanath, Adam Kaminski. Intrinsic axion insulating behavior in antiferromagnetic $\text{MnBi}_6\text{Te}_{10}$. arXiv:1910.14626 (2019).
59. Hideaki Iwasawa, Eike F. Schwier, Masashi Arita, Akihiro Ino, Hirofumi Namatame, Masaki Taniguchi, Yoshihiro Aiura, Kenya ShimadaIwasawa, H. et al. Development of laser-based

scanning micro-ARPES system with ultimate energy and momentum resolutions. *Ultramicroscopy* **182**, 85 (2017).

60. Chaoyu Chen, Zhuojin Xie, Ya Feng, Hemian Yi, Aiji Liang, Shaolong He, Daixiang Mou, Junfeng He, Yingying Peng, Xu Liu, Yan Liu, Lin Zhao, Guodong Liu, Xiaoli Dong, Jun Zhang, Li Yu, Xiaoyang Wang, Qinjun Peng, Zhimin Wang, Shenjin Zhang, Feng Yang, Chuangtian Chen, Zuyan Xu and X. J. Zhou, Tunable Dirac fermion dynamics in topological insulators. *Sci. Rep.* **3**, 2411 (2013).
61. I.I. Klimovskikh, M. M. Otrokov, D. Estyunin, S.V. Eremeev, S.O. Filnov, A. Koroleva, E. Shevchenko, V. Voroshnin, I.P. Rusinov, M. Blanco-Rey, M. Hoffmann, Z.S. Aliev, M.B. Babanly, I.R. Amiraslanov, N.A. Abdullayev, V.N. Zverev, A. Kimura, O.E. Tereshchenko, K. A. Kokh, L. Petaccia, G. Di Santo, A. Ernst, P.M. Echenique, N.T. Mamedov, A.M. Shikin and E. V. Chulkov, Variety of magnetic topological phases in the $(\text{MnBi}_2\text{Te}_4)(\text{Bi}_2\text{Te}_3)_m$ family. arXiv:1910.11653 (2019).
62. G. Kresse, J. Furthmüller, Efficient iterative schemes for ab initio total-energy calculations using a plane-wave basis set. *Phys. Rev. B*, **54**, 11169 (1996).
63. G. Kresse, J. Furthmüller. Efficiency of ab-initio total energy calculations for metals and semiconductors using a plane-wave basis set. *Comp. Mater. Sci.* **6**, 15 (1996).
64. P. Hohenberg and W. Kohn. Inhomogeneous electron gas. *Phys. Rev.* **136**, B864 (1964).
65. W. Kohn and L. J. Sham, Self-consistent equations including exchange and correlation effects. *Phys. Rev.* **140**, A1133 (1965).
66. John P. Perdew, Kieron Burke, Matthias Ernzerhof. Generalized gradient approximation made simple. *Phys. Rev. Lett.* **77**, 3865 (1996).
67. P. E. Blöchl, Projector augmented-wave method. *Phys. Rev. B* **50**, 17953 (1994).
68. G. Kresse and D. Joubert, From ultrasoft pseudopotentials to the projector augmented-wave method. *Phys. Rev. B* **59**, 1758 (1999).
69. Hendrik J. Monkhorst and James D. Pack, Special points for Brillouin-zone integrations. *Phys. Rev. B* **13**, 5188 (1976).
70. A. I. Liechtenstein, V. I. Anisimov, J. Zaanen, Density-functional theory and strong interactions: Orbital ordering in Mott-Hubbard insulators. *Phys. Rev. B* **52**, R5467 (1995).
71. M M Otrokov, T V Menshchikova, M G Vergniory, I P Rusinov, A Yu Vyzovskaya, Yu M Koroteev, G Bihlmayer, A Ernst, P M Echenique, A Arnau and E V Chulkov. Highly-ordered wide bandgap materials for quantized anomalous Hall and magnetoelectric effects. *2D Mater.* **4**(2), 025082 (2017).
72. Liang Fu and Erez Berg, Odd-Parity topological superconductors: Theory and application to $\text{Cu}_x\text{Bi}_2\text{Se}_3$. *Phys. Rev. Lett.* **105**, 097001 (2017).